Nanoscale

PAPER

View Article Online
View Journal | View Issue

Check for updates

Cite this: *Nanoscale*, 2023, **15**, 9049

Sulfidation and NaOH etching in CoFeAl LDH evolved catalysts for an efficient overall water splitting in an alkaline solution†

Xiaolong Deng, *[a] Shanshan Wang,[a] Yi Liu,[a] Jiafeng Cao,*[a] Jinzhao Huang *[b] and Xingwei Shi [c]

In this study, a hierarchical interconnected porous metal sulfide heterostructure was synthesized from CoFeAl layered double hydroxides (LDHs) by a two-step hydrothermal process (sulfidation and a NaOH etching process). Among the as-made samples, the CoFeAl-T-NaOH electrode exhibited excellent oxygen and hydrogen evolution reaction catalytic activities with overpotentials of 344 mV and 197 mV at the current density of 100 mA cm^{-2}, respectively. Meanwhile, small Tafel slopes of 57.7 mV dec^{-1} and 106.5 mV dec^{-1} for water oxidation and hydrogen evolution were observed for the CoFeAl-T-NaOH, respectively. Serving as both the cathode and anode for overall water splitting, the CoFeAl-T-NaOH electrode reached a current density of 10 mA cm^{-2} at a cell voltage of 1.65 V with excellent stability. The enhanced electrocatalytic activity could be attributed to: the hierarchical interconnected nanosheet structure facilitating mass transport; the porous structure promoting electrolyte infiltration and reactant transfer; the heterojunction accelerating charge transfer; and the synergistic effect between them. This study offered a new clue for *in situ* synthesizing porous transition-metal based heterojunction electrocatalysts with a careful tuning of the sequence of sulfuration and alkaline etching to enhance the electrocatalytic performance.

Received 20th March 2023,
Accepted 25th April 2023

DOI: 10.1039/d3nr01276j

rsc.li/nanoscale

Published on 25 abril 2023. Downloaded on 06/07/2024 19:31:19.

1. Introduction

The development of green energy and a sustainable energy system is essential to alter the use of transitional fossil fuel resources in response to the worldwide environmental and energy crises.[1] Oxygen and hydrogen generated from water splitting has been considered one of the most promising approaches for electrochemical energy storage and conversion.[2] The involved two half-reactions, the hydrogen evolution reaction (HER) and oxygen evolution reaction (OER), were driven by the theoretically thermodynamic overpotentials of 0 V and 1.23 V respectively.[3,4] However, there still remain challenges for the practical application due to the much higher overpotential and unclear underlying mechanism. Therefore, the development of an efficient electrocatalysts is a promising approach to achieve a high current density at a relatively low overpotential.[5] In order to lower the overpotential, many efforts have been made, including catalyst selection, structure design and regulation.[2,6–10] The development of non-precious metal based electrocatalysts with a high activity and durability has the potential for large-scale practical applications.[11] Among these, transition-metal based layered double hydroxides (LDHs) have attracted tremendous interest due to their unique structure and physicochemical properties.[12–14] However, their practical applications were limited due to the poor conductivity and easy aggregation of LDHs.[15] Thus, many efforts have been made to further improve the electrochemical performance of LDHs by tuning the species and the molar ratio of metal cations, exchanging the interlayer anions, expanding the interlayer distance, and anchoring metal atoms and modulating defects in the layered structure and so on.[12,16–19]

Among these modification approaches, the generation of LDH derivatives was one of the most promising clues to enhance the electrocatalytic properties.[20,21] For example, Fu *et al.* had successfully synthesized anion-modulated 3D Ni–V based transition metal interstitial compound (TMIC) heterojunctions on nickel foam through a hydrothermal method followed by a phosphorization treatment. It was demonstrated that the excellent water splitting performance could be ascribed to the heterointerfaces, good conductivity, intimate

[a]*School of Microelectronics and Data Science & Institute of Optoelectronics and New Energy, Anhui University of Technology, Ma'anshan 243032, Anhui Province, P. R. China. E-mail: dengxl84@ahut.edu.cn, jiafengcao@126.com*
[b]*School of Physics and Technology, University of Jinan, Jinan 250022, Shandong Province, P. R. China. E-mail: ss_huangjinzhao@ujn.edu.cn*
[c]*Beijing Key Laboratory of Ionic Liquids Clean Process, CAS Key Laboratory of Green Process and Engineering, Institute of Process Engineering, Chinese Academy of Sciences, Beijing 100190, China*

†Electronic supplementary information (ESI) available. See DOI: https://doi.org/10.1039/d3nr01276j

Published on 25 abril 2023. Downloaded on 06/07/2024 19:31:19.

contact, and porous structure.[22] It was reported that Co_3S_4/Fe_3S_4 heterostructures on nickel foam evolved from CoFe LDH by a two-step hydrothermal method has an outstanding bifunctional catalytic performance due to the interconnected structure and a synergistic effect.[23] Moreover, transition-metal chalcogenides have been widely investigated due to their excellent electrocatalytic performance partially induced by the porous structures and heterostructures.[24–27] Sulfur was incorporated into NiFe (oxy)hydroxide (S-NiFeOOH) grown on nickel foam by a galvanic corrosion method and a hydrothermal method and showed an enhanced overall water splitting activity, which was attributed to the change in the local structure and chemical states.[28] In other words, the formation of heterojunctions and sulfurization could enhance the electrocatalytic activities.

Recently, the NaOH etching effect was also investigated to improve the electrocatalytic activity. For example, a NaOH-assisted thioacetamide etching strategy was also applied to prepare a hollow nanostructured ZIF bimetallic sulfide with enhanced OER/HER catalytic activities.[29] Most importantly, the amphoteric Al in LDH could be selectively etched by an alkaline solution to construct a porous structure, favorable for the electrocatalytic performance. Wang *et al.* reported that the CoAl LDH etched by a NaOH solution accompanied by sulfurization and phosphorization as the electrocatalyst exhibited outstanding OER and HER performances.[30,31] In addition, different etchants, such as NaOH and HF, were used to investigate the etching effect of the catalysts.[32] However, few reports studied the electrocatalytic performance of metal LDH *via* a sequential sulfidation and NaOH etching process.

Herein, a facile two-step hydrothermal approach was applied to synthesize bifunctional overall water splitting electrocatalysts derived from CoFeAl LDH through sulfidation and NaOH etching with a reverse sequence (named as CoFeAl-T-NaOH and CoFeAl-NaOH-T). Among these, the best CoFeAl-T-NaOH electrode showed excellent OER and HER performances with overpotentials of 343 mV and 197 mV to deliver 100 mA cm^{-2} and Tafel slopes of 57.7 mV dec^{-1} and 106.5 mV dec^{-1}, respectively. In addition, CoFeAl-T-NaOH reached a current density of 10 mA cm^{-2} for the overall water splitting at a cell voltage of 1.65 V with excellent stability. The enhanced electrocatalytic activity could be ascribed to the interconnected hierarchical structure, nanopores and heterostructures for accelerated mass transport, product diffusion and charge transfer. This work proposes a new strategy to synthesize porous structures of transition-metal chalcogenide heterostructures from LDHs and emphasizes the importance of the synthesis sequence for an enhanced electrocatalytic performance.

2. Experimental section

2.1. Materials

Cobalt chloride hexahydrate ($CoCl_2{\cdot}6H_2O$), iron chloride hexahydrate ($FeCl_3{\cdot}6H_2O$), aluminum chloride hexahydrate ($AlCl_3{\cdot}6H_2O$), ammonium fluoride (NH_4F), urea (CH_4N_2O), thiourea (CH_4N_2S), 5.0 M sodium hydroxide analytical titrant (NaOH), and 1.0 M potassium hydroxide analytical titrant (KOH) were purchased from Shanghai Aladdin Biochemical Technology Co., Ltd. Absolute ethanol (C_2H_6O) was obtained from Sinopharm Chemical Reagent Co., Ltd. All the chemical reagents were analytical grade and used as received without further purification.

2.2. Preparation of the CoFeAl LDH precursor

The nickel foam was treated ultrasonically with deionized water and ethanol for 5 min each, and then dried in a vacuum oven at 60 °C for 12 h. The CoFeAl LDH precursor was hydrothermally *in situ* grown on the Ni foam with a typical procedure depicted as follows: first, the homogeneous solution was prepared by mixing 0.8 mmol $CoCl_2{\cdot}6H_2O$, 0.4 mmol $FeCl_3{\cdot}6H_2O$, 0.4 mmol $AlCl_3{\cdot}6H_2O$, 4 mmol NH_4F, and 28 mmol urea in 40 mL of deionized water and stirred for 30 min. Then, the above solution was transferred into a 50 mL Teflon-lined stainless steel autoclave with several pieces of Ni foam (size of 1 cm × 2 cm) and kept in an oven at 100 °C for 6 hours. After cooling down to room temperature naturally, the products grown on the Ni foam were cleaned by deionized water and absolute ethanol several times. Finally, the CoFeAl LDH precursor was obtained by drying at 60 °C for 12 hours in a vacuum oven.

2.3. Synthesis of the CoFeAl-T-NaOH catalyst

First, the CoFeAl LDH precursor was placed in an autoclave with 40 mL of aqueous solution containing 0.6 mmol thiourea and reacted at 140 °C for 5 h. After cooling to room temperature naturally, the product was washed with deionized water and ethanol, and dried at 60 °C for 12 hours in a vacuum to obtain the CoFeAl-T catalyst. Then, the CoFeAl-T sample was immersed in 30 ml of NaOH solution and transferred into a 50 mL Teflon-lined stainless steel autoclave. After keeping at 120 °C for 12 hours and then cooling down naturally to room temperature, the sample was washed by ethanol and deionized water followed by drying to obtain the CoFeAl-T-NaOH catalyst.

In addition, blank nickel foam (size of 1 cm × 2 cm) was vulcanized by 40 mL of aqueous solution containing only 0.6 mmol thiourea in the autoclave at 140 °C for 5 hours, followed by naturally cooling to room temperature, washing with deionized water and ethanol, and drying in a vacuum oven at 60 °C for 12 hours to obtain Ni foam-T as a control sample.

2.4. Synthesis of the CoFeAl-NaOH-T catalyst

The CoFeAl LDH precursor was put into 30 ml of a 5.0 M NaOH solution and then transferred into a 50 mL Teflon-lined stainless steel autoclave. After reacting at 120 °C for 12 h and cooling to room temperature naturally, the product was washed with deionized water and ethanol, and dried at 60 °C for 12 hours in a vacuum to obtain the CoFeAl-NaOH. Then, the CoFeAl-NaOH was transferred into an autoclave along with 40 mL of aqueous solution containing 0.6 mmol thiourea (T)

 This journal is © The Royal Society of Chemistry 2023

Published on 25 abril 2023. Downloaded on 06/07/2024 19:31:19.

and kept at 140 °C for 5 hours. After washing and drying, the CoFeAl-NaOH-T catalyst was obtained.

2.5. Characterization

The structures of the as-prepared samples were characterized by an X-ray diffractometer (Bruker D8 Advance diffractometer) equipped with a monochromatic Cu Kα radiation (λ = 0.15406 nm). The morphologies and microstructures of the as-prepared samples were observed by a JEOL JSM-6700F scanning electron microscope (SEM) coupled with an energy-dispersive X-ray spectroscope (EDS) and transmission electron microscope (TEM, JEOL JEM-3000F). The surface chemical oxidation states of the samples were recorded by X-ray photoelectron spectroscopy (XPS) using a Thermo Scientific ESCALAB Xi+ spectrometer equipped with a monochromatic Al Kα X-ray source (1486.6 eV). All the XPS peaks were calibrated with a C 1s peak binding energy at 284.8 eV for adventitious carbon.

2.6. Electrochemical measurement

The electrochemical measurement was carried out on an electrochemical workstation (CHI 760E, Chenhua, Shanghai, China) at room temperature with 80 mL of a 1.0 M KOH aqueous solution as the electrolyte. A traditional three-electrode cell was assembled by employing an Ag/AgCl reference electrode, a carbon rod counter electrode and the electrocatalyst used as the working electrode. In addition, all the potentials measured with the three-electrode system were calibrated to a reversible hydrogen electrode (RHE), according to the following equation:

$$E_{vs.\ \mathrm{RHE}} = E_{\mathrm{Ag/AgCl}} + 0.198\ \mathrm{V} + 0.059 \times \mathrm{pH}. \quad (1)$$

The linear sweep voltammetry (LSV) was evaluated at a sweep rate of 10 mV s^{-1} with a 95% iR compensation. The samples were activated by scanning the cyclic voltammogram (CV) for 20 cycles to reach the stable state with a scan potential range from 1.1 to 1.8 V (*vs.* RHE) for OER and from −0.5 to 0 V (*vs.* RHE) for HER. Electrochemical impedance spectroscopy (EIS) was recorded with a frequency range from 0.01 Hz to 100 kHz and an amplitude of 5 mV. A chronopotentiometric curve was collected at a current density of 150 mA cm^{-2} to evaluate the electrochemical stability of the electrocatalysts. The CVs, from 0.948 to 1.1 V (*vs.* RHE) for OER, were collected at scan rates of 40, 60, 80, 100, 120, 140, 160, 180 and 200 mV s^{-1} to estimate the double layer capacitance (C_{dl}),[21] which was used to appraise the electrochemical surface area (ECSA). The ECSA was estimated from a linear plot of the charging current density at 1.024 V (*vs.* RHE) *versus* the scan rate. The current density was obtained according to

$$\Delta j = j_a - j_b. \quad (2)$$

3. Results and discussion

3.1. Structural and morphological characterization

The as-prepared samples show strong characteristic peaks at 44.7°, 52.1° and 76.5°, which are indexed to the (111), (200) and (220) planes of Ni (JCPDS no. 70-1849) from the Ni foam substrate (Fig. 1 and Fig. SI1†). For the CoFeAl LDH pre-catalyst (Fig. SI1a and b†), the peaks at 11.8°, 23.4°, 34.5°, 39.1° and 46.8° are assigned to the (003), (006), (012), (015) and (018) planes (JCPDS no. 25-0521).[33–35] After NaOH etching, the characteristic peaks of CoFeAl LDH disappeared (Fig. SI1a†), which is consistent with a previous report.[30] Meanwhile, the XRD pattern of the sample generated by the sulfidation treatment of CoFeAl LDH is recorded in Fig. SI1a and c† (named as CoFeAl-T). As can be seen, besides the three strong peaks from the Ni foam substrate and the remaining CoFeAl LDH reflections, the newly appeared peaks are assigned to (220), (311), (400), (511) and (440) of Co_3S_4 (JCPDS no. 42-1448), (222), (422) and (440) of Fe_3S_4 (JCPDS no. 16-0713), (101), (110), (003), (202), (113) and (300) of Ni_3S_2 (JCPDS no. 44-1418), and (222), (400), (511) and (440) of Al_2S_3 (JCPDS no. 26-0037).[23,36–38] However, after sulfidation and NaOH etching (CoFeAl-NaOH-T and CoFeAl-T-NaOH), the characteristic reflections of Al_2S_3 from XRD patterns disappeared, leaving only the Co_3S_4, Fe_3S_4, and Ni_3S_2 reflections (Fig. 1a and b). This confirmed the successful sulfidation and etching of the Al element from CoFeAl LDH[30] with a heterostructure.[23] Furthermore, by changing the

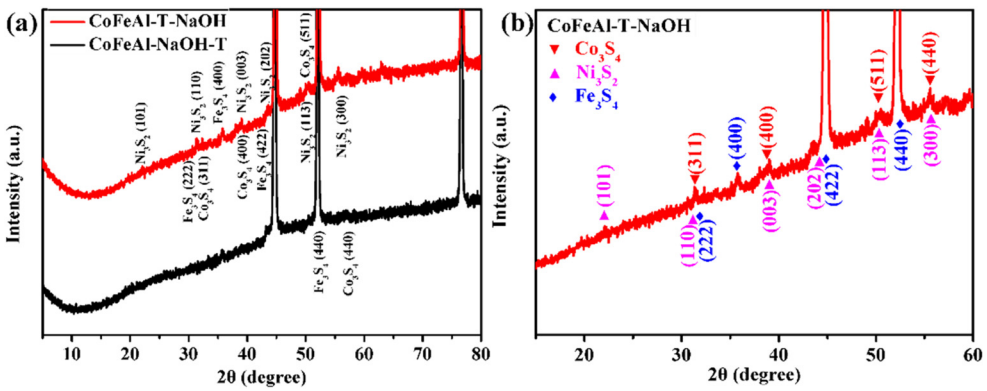

Fig. 1 (a) XRD patterns of the samples: CoFeAl-NaOH-T and CoFeAl-T-NaOH, (b) the enlarged XRD pattern of CoFeAl-T-NaOH.

Published on 25 abril 2023. Downloaded on 06/07/2024 19:31:19.

sequence of sulfidation and NaOH etching, the intensities of the XRD patterns were varied, which affects the structure of the as-prepared samples (in Fig. 1 and Fig. SI1,† see below).

The scanning electron microscopy (SEM) micrographs were investigated to show the morphological structures of the samples. The sphere-like structure is composed of interconnected nanosheets with a thickness of ~100 nm for the Ni foam-T sample (Fig. SI2a and b†), and the Ni and S elements are homogeneously distributed (Fig. SI2c†). For the CoFeAl LDH precursor, similar spheres are formed with rough surface, composing interconnected nanosheets with thickness of ~70 nm (Fig. SI2d and e†) and uniformly distributed Co, Fe, and Al elements (Fig. SI2f†). After etching with NaOH, the sample CoFeAl-NaOH showed the porously wrinkled film structure (Fig. SI2g†). The enlarged SEM image showing the films were composed of nanosheets with a homogeneous distribution of the Co and Fe elements (Fig. SI2h and i†), demonstrating that NaOH etching helps the generation of a porous structure. However, the sulfidation of CoFeAl LDH (CoFeAl-T) formed the interconnected dense flakes with a thickness of ~20 nm and a smooth surface (Fig. SI2j and k†) and the Co, Fe, Al and S elements were homogeneously distributed (Fig. SI2l†), elucidating that the sole sulfidation process also varied the morphological structure. Furthermore, by treating with NaOH etching and sulfidation one after another, the morphology of CoFeAl-NaOH-T exhibited a dense nanosheet structure composed of nanoparticles with destructured irregular pores and a homogeneous distribution of the Co, Fe, S and Ni elements. However, the CoFeAl-T-NaOH morphology changed significantly compared with that of CoFeAl-NaOH-T. As shown in Fig. 2d–f, CoFeAl-T-NaOH shows a porous film structure composed of interconnected nanosheets. In addition, the interconnected nanosheets comprise nanoparticles with homogenously distributed Co, Fe, S and Ni elements. Moreover, the molar ratio of Co : Fe : S was estimated to be 1.7 : 1.9 : 1 for CoFeAl-T-NaOH and 1.0 : 1.4 : 10 for CoFeAl-NaOH-T by SEM-EDS analysis. The porous structure of the as-prepared electrocatalysts has the advantage that it promotes electrolyte diffusion and mass transfer, resulting in an enhancement of the electrocatalytic activity (see below).

The morphology of the as-prepared samples was further investigated by transmission electron microscopy (TEM). The CoFeAl LDH sample in Fig. SI3a† exhibits an interconnected flake-like structure and a lattice fringe of 0.198 nm was

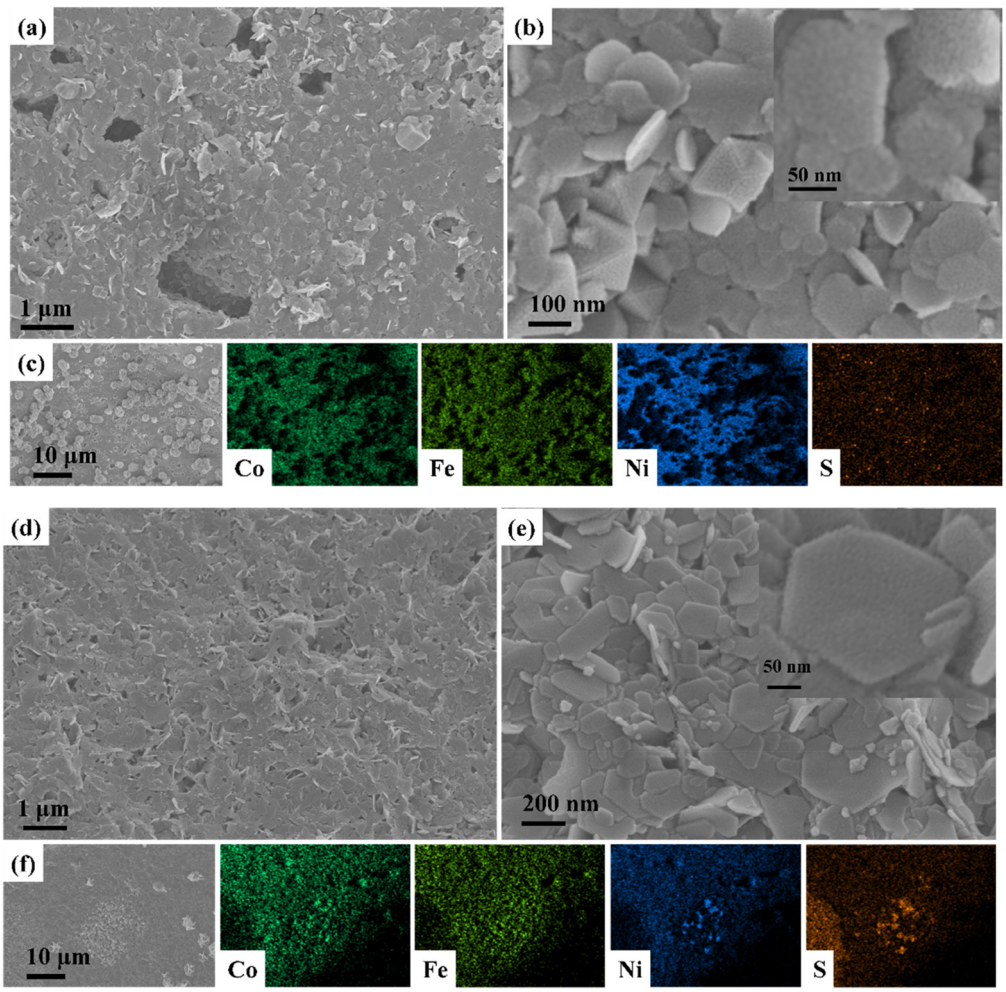

Fig. 2 SEM images and corresponding elemental mapping images of the as-prepared samples: CoFeAl-NaOH-T (a–c) and CoFeAl-T-NaOH (d–f).

 This journal is © The Royal Society of Chemistry 2023

observed by HRTEM (Fig. SI3b†), matching well with the (018) plane of CoFeAl LDH.[33–35] After NaOH etching (CoFeAl-NaOH), the morphology evolves to nanosheets formed porous structure (Fig. SI3d and e†). Moreover, CoFeAl-T depicts dense flakes constructed of a hierarchically interconnected structure (Fig. SI3g and h†). All the samples show a homogeneous elemental distribution (Fig. SI3c, f and i†). Fig. 3a exhibits the dense flake structure of CoFeAl-NaOH-T, in good consistency with the SEM observation. The HRTEM of CoFeAl-NaOH-T shows *d*-spacing distances of 0.236, 0.202 and 0.205 nm, corresponding to the (400), (422) and (202) crystalline planes of Co_3S_4, Fe_3S_4 and Ni_3S_2, respectively (Fig. 3b), indicating the formation of the metal sulfide heterostructures of $Co_3S_4/Fe_3S_4/Ni_3S_2$. The EDS mapping (Fig. 3c) shows a uniform distribution of the Co, Fe, Ni and S elements over CoFeAl-NaOH-T. In comparison, the CoFeAl-T-NaOH is made up of interconnected porous nanosheets which are assembled by the nanoparticles (Fig. 3d) contributing to the hierarchical porous nanostructure. The lattice fringes of 0.236, 0.247 and 0.204 nm, correspond to the (400), (400) and (202) crystalline planes of Co_3S_4, Fe_3S_4 and Ni_3S_2, respectively (Fig. 3e), showing the formation of a metal sulfide heterostructure. In addition, the EDS elemental mapping confirms the homogeneous distribution of the Co, Fe, Ni and S elements over CoFeAl-T-NaOH (Fig. 3f). In addition, the content of Al in the different catalysts was evaluated by the molar ratio Fe/Al through a TEM-EDS analysis, as

Published on 25 abril 2023. Downloaded on 06/07/2024 19:31:19.

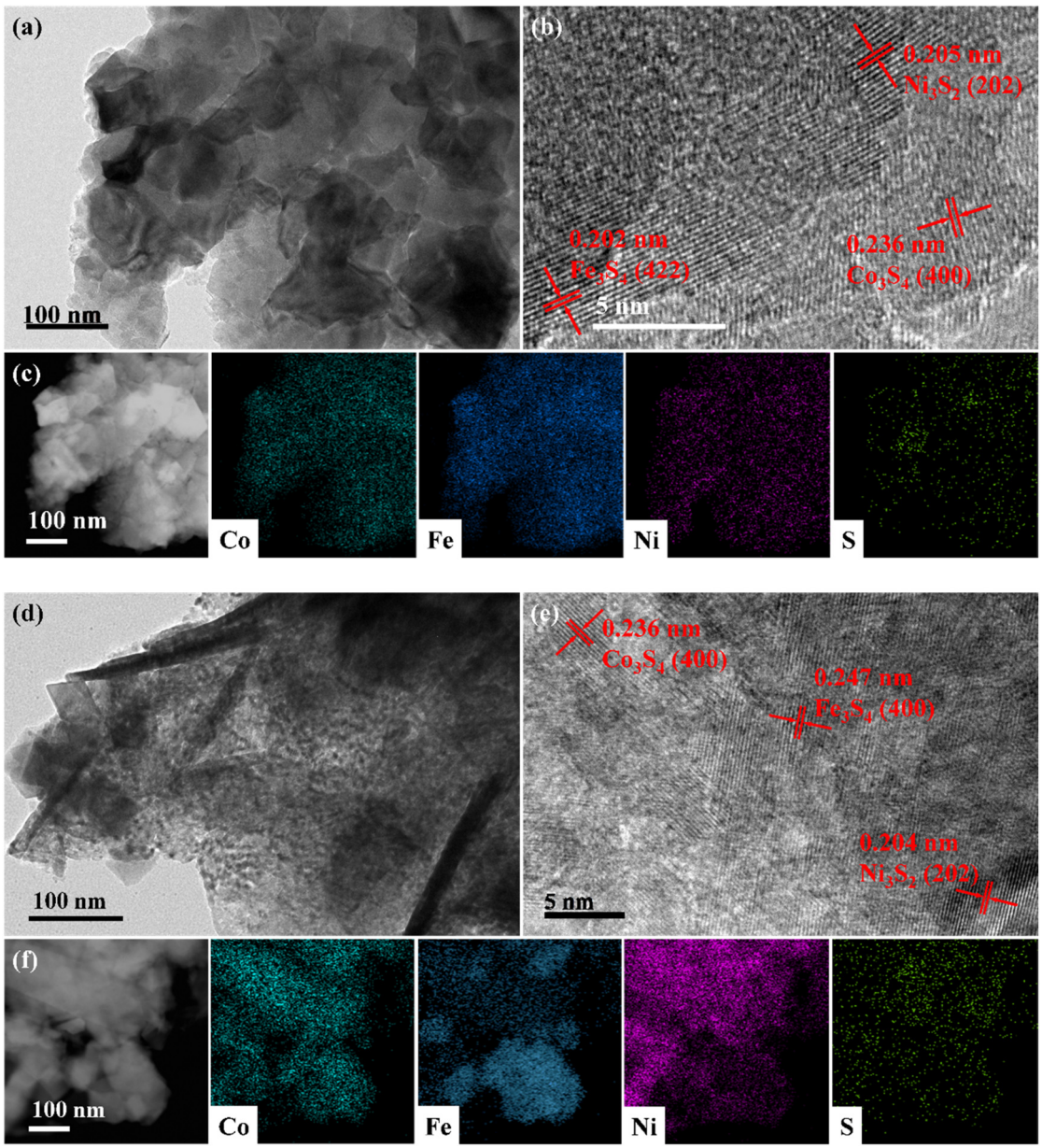

Fig. 3 TEM image, HRTEM image and corresponding elemental mapping image of the as-synthesized samples: CoFeAl-NaOH-T (a–c) and CoFeAl-T-NaOH (d–f).

Published on 25 abril 2023. Downloaded on 06/07/2024 19:31:19.

shown in Table SI1,† demonstrating the almost complete removal of Al with NaOH etching. Comparison of the TEM observations for CoFeAl-NaOH-T and CoFeAl-T-NaOH elucidates the effect of the sequence of sulfidation and NaOH etching on the morphological structure (Fig. 3a and d).

Fig. 4 and Fig. SI4† depict the XPS spectra to further analyze the surface chemical oxidation states of the samples. From Fig. SI4a,† the XPS survey spectrum shows the elements Co, Fe, Al, Ni, and O for the CoFeAl LDH sample, demonstrating the successful growth of CoFeAl LDH on nickel foam.[5] Moreover, the disappearance of the signal of the Al element in CoFeAl-NaOH illustrates the successful etching of Al (Fig. SI4a†), which is consistent with the elemental mapping change of Al (Fig. SI3c and f†) with the molar ratio of Fe/Al changing from 3.9 : 1 to 6.1 : 1. The Co 2p and Fe 2p XPS core spectra (Fig. SI4b and c†) for CoFeAl-NaOH and CoFeAl LDH exhibit similar curves, elucidating the non-destructive NaOH etching for the Co and Fe components in CoFeAl LDH. For CoFeAl-T, there is no change for the survey and core spectrum of Al (Fig. 4a and SI4d†), except for the appearance of the S element in CoFeAl-NaOH, confirming the successful sulfidation. Meanwhile, the high-resolution Al 2p XPS spectra of CoFeAl LDH and CoFeAl-T in Fig. SI4d† show a pair of peaks at 68.8 eV (Al $2p_{3/2}$) and 73.5 eV (Al $2p_{1/2}$), indicating the existence of Al^{3+}.[5] From Fig. 4a, the XPS survey spectra show the elements of Co, Fe, Ni, and S for CoFeAl-T, CoFeAl-T-NaOH, and CoFeAl-NaOH-T, demonstrating the formation of metal sulfides by a sulfidation process. The high-resolution Co 2p XPS spectra (Fig. 4b) show a pair of peaks at binding energies of ~781.2 eV (Co $2p_{3/2}$) and ~797.8 eV (Co $2p_{1/2}$), with two satellite peaks at ~784.8 eV and ~803.2 eV, demonstrating the existence of Co^{2+}.[39–41] In Fig. 4c, the high-resolution Fe 2p XPS spectra are deconvoluted to give two major peaks located at 711.1 eV (Fe $2p_{3/2}$) and 724.5 eV (Fe $2p_{1/2}$) with two satellite peaks located at 716.4 eV and 732.5 eV, demonstrating the existence of Fe^{3+}.[40,42] After sulfidation and/or NaOH etching process, both the Co 2p and Fe 2p core spectra show a slight down-shift compared with that of CoFeAl LDH (Fig. SI4b and c†), indicating the higher valence of Co (Co^{3+}) and the lower-valence state of Fe (Fe^{2+}).[42–44] The high-resolution S 2p XPS spectra in Fig. 4d and Fig. SI4d† show two main peaks at the binding energies of 162.5 eV and 168.8 eV, corresponding to unsaturated S^{2-} and S^{6+} (S═O), being favorable for the electrocatalytic process.[45,46]

3.2. OER catalytic performance

The OER performance was evaluated through a three-electrode system at room temperature in 1.0 M KOH with a scanning speed of 10 mV s^{-1}. From the linear sweep voltammetry curves (LSV) in Fig. 5a, the CoFeAl-T-NaOH catalyst shows the lowest overpotential of 344 mV to reach a current density of 100 mA cm^{-2}, which is much lower than those of 367 mV, 373 mV, 390 mV, 401 mV and 415 mV for CoFeAl-T, CoFeAl-NaOH, CoFeAl-NaOH-T, CoFeAl LDH and Ni foam-T, respectively. In addition, the overpotential of CoFeAl-T-NaOH only increased to 368 mV at 300 mA cm^{-2}, manifesting its potential for high current catalytic applications. The Tafel slopes were calculated

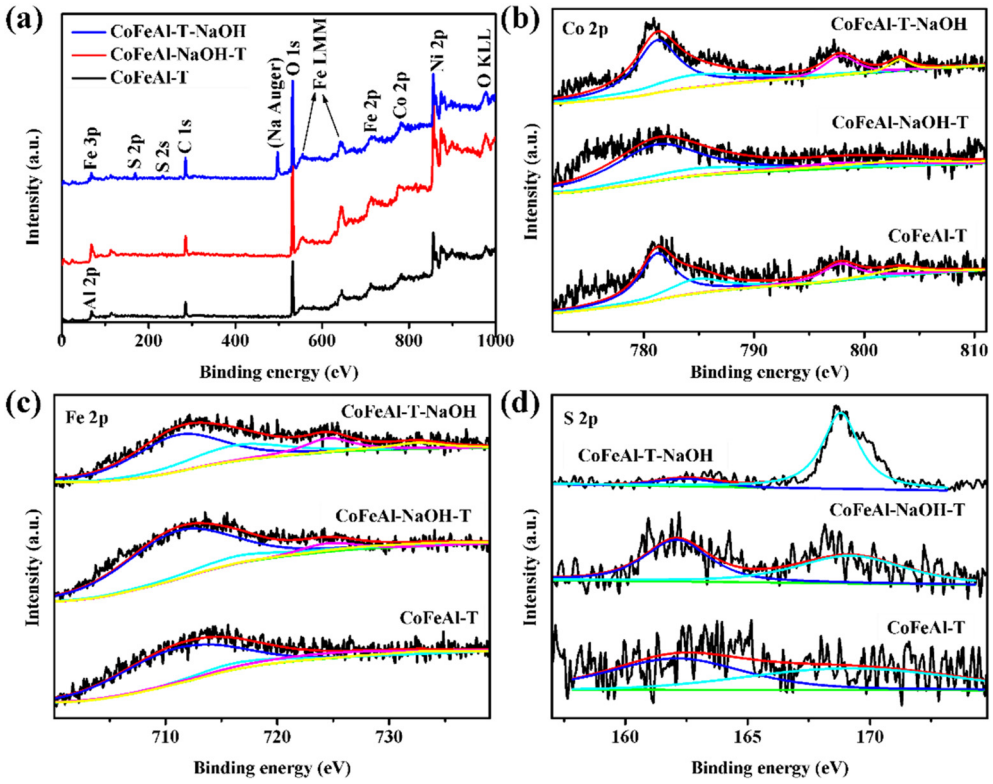

Fig. 4 XPS analysis of the as-prepared samples: XPS survey spectra (a), high-resolution spectra of (b) Co 2p, (c) Fe 2p and (d) S 2p.

This journal is © The Royal Society of Chemistry 2023

Published on 25 abril 2023. Downloaded on 06/07/2024 19:31:19.

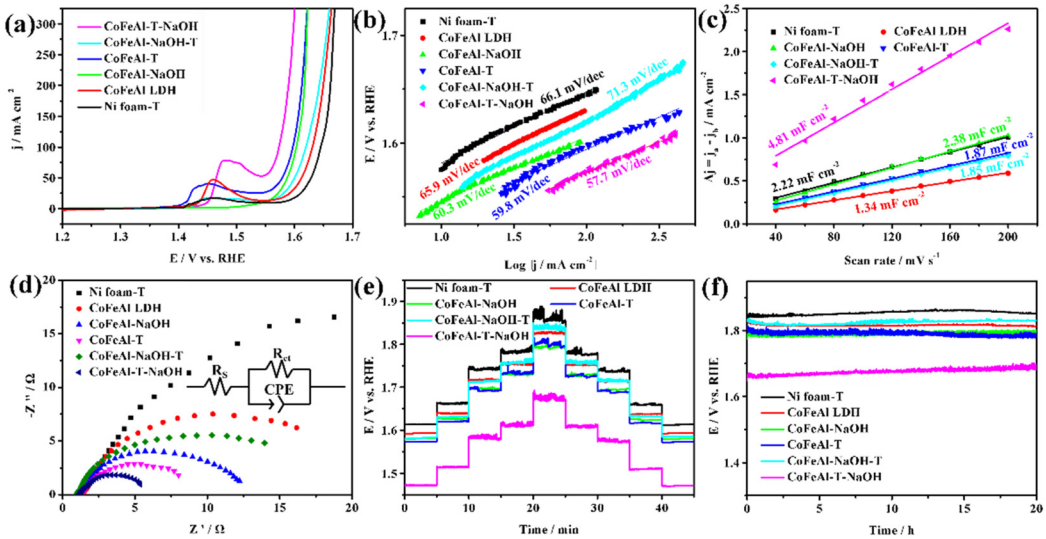

Fig. 5 The electrochemical performance of the as-synthesized samples for OER: (a) the polarization curves with 95% iR compensation. (b) The corresponding Tafel plots. (c) ECSA values for the as-made catalysts. (d) Nyquist plots measured at 1.55 V (*vs.* RHE); the inset is the equivalent circuit of the EIS. (e) Multistep chronopotentiometry response without iR compensation with current densities of 10, 30, 75, 100 and 150 mA cm^{-2}. (f) Chronopotentiometric curves of the as-prepared catalysts measured at 150 mA cm^{-2} for 20 hours.

from the polarization curves and are plotted in Fig. 5b. The CoFeAl-T-NaOH electrode shows the smallest Tafel slope of 57.7 mV dec^{-1}, demonstrating its fast reaction kinetics.[45] Furthermore, electrochemical surface area (ECSA), usually used to reveal the catalytic mechanism, was estimated by measuring the double layer capacitance (Fig. SI5†). As seen in Fig. 5c, the CoFeAl-T-NaOH has the largest ECSA value, illustrating more exposed catalytic active sites.[47]

Similarly, electrochemical impedance spectroscopy (EIS) was adopted to estimate the electrical conductivity of the electrocatalyst. Nyquist plots were fitted using the equivalent circuit of $R(Q(R))$ (Fig. 5d), where R_S, R_{ct} and CPE represent the solution resistance, charge transfer resistance and constant phase element, respectively.[23,48] The R_{ct} values of the electrocatalysts were estimated to be 5.03, 8.04, 11.25, 15.61, 20.22 and 53.88 Ω for CoFeAl-T-NaOH, CoFeAl-T, CoFeAl-NaOH, CoFeAl-NaOH-T, CoFeAl LDH and Ni foam-T, respectively. Therefore, the CoFeAl-T-NaOH catalyst has the smallest charge transfer resistance, exhibiting a fast charge transfer capability among the synthesized catalysts. The small charge transfer resistance of CoFeAl-T-NaOH may be ascribed to the synergistic effect of the heterostructure, interconnected structure and porous structure, offering more conductive and numerous active sites, which is favorable for electrolyte ion filtration and thus facilitate charge transfer.[19]

Furthermore, multistep chronopotentiometry was used to investigate the mass transfer capability and stability of the as-made catalysts. Fig. 5e shows the multistep chronopotentiometry curves with the current density increasing from 10 to 150 mA cm^{-2} at a time interval of 5 min. Each step exhibits an abrupt response of the OER potential and is steady without fluctuation, indicating an outstanding mass transport and charge transfer performance. Furthermore, the long-term stability was assessed by measuring the potential at a current density of 150 mA cm^{-2} (Fig. 5f). A stable curve without a detectable degradation was recorded, illustrating the long-term robustness of CoFeAl-T-NaOH. The XRD pattern, SEM observation and XPS spectra after long-term OER measurement were further studied to prove the stability of the catalyst. The XRD pattern remains almost constant as the pristine CoFeAl-T-NaOH (Fig. SI6a†) and SEM image exhibit a slight morphology change (Fig. SI6b–d†), confirming the stable activity of the electrocatalyst. The XPS survey spectrum, and XPS data of Co 2p and Fe 2p, exhibit no significant difference before and after the long-term test (Fig. SI7a–c†). However, Fig. SI7d† depicts a weakened peak at 162.5 eV after the OER test, suggesting a partially oxidized S element during the OER process.[23,37] The high resolution XPS spectrum of O 1s (Fig. SI7e†) shows peaks at 530.8 eV, 531.5 eV and 532.3 eV, corresponding to lattice oxygen, oxygen defects and adsorbed oxygen species, respectively, indicating the existence of metal oxides on the surface due to the unavoidable electrochemical oxidation.[30,49] These results confirm that the metal oxides are the true active sites for OER. In other words, the CoFeAl-T-NaOH catalyst exhibits an outstanding and stable OER catalytic performance, which is ascribed to the porous structure offering more exposed active sites, the interconnected structure facilitating mass transport, and the heterojunction accelerating charge transfer and enhancing the synergistic effect.

3.3. HER catalytic performance

The hydrogen evolution reaction (HER) performance of the as-prepared catalysts was also investigated. The CoFeAl-T-NaOH catalyst possesses the smallest overpotential (197 mV) at a current density of 100 mA cm^{-2}, which merely increased to 237 mV at 300 mA cm^{-2} (Fig. 6a). Moreover, the Tafel slope

Published on 25 abril 2023. Downloaded on 06/07/2024 19:31:19.

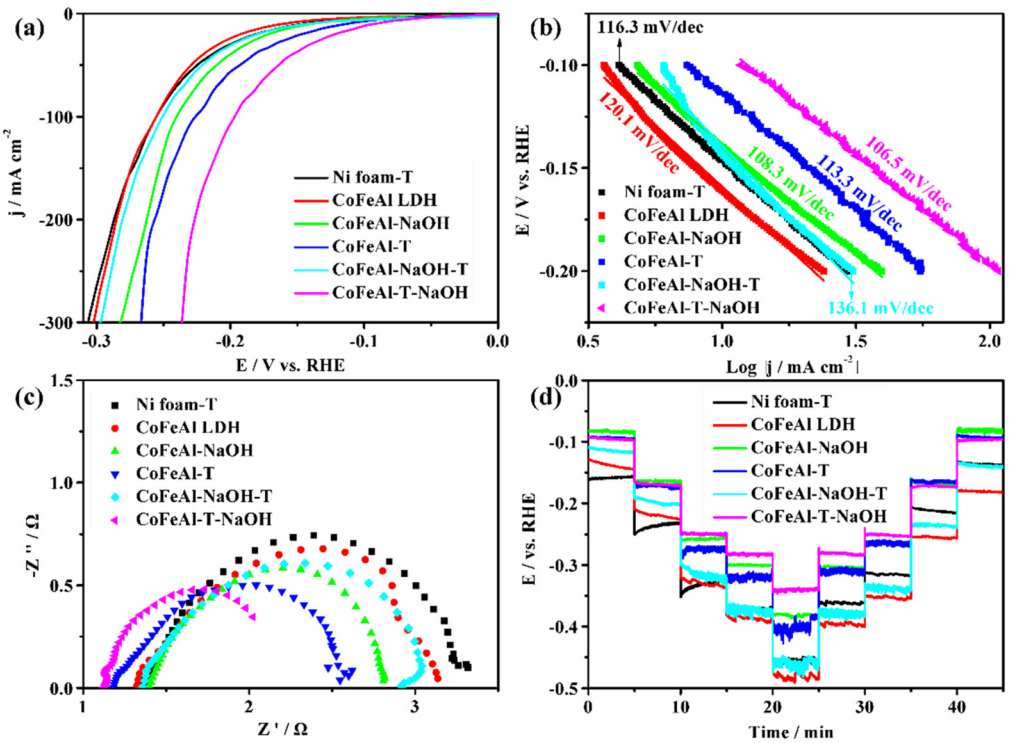

Fig. 6 HER catalytic performances of the as-synthesized samples: (a) LSV curves at a scan rate of 10 mV s^{-1} with a 95% iR compensation. (b) The corresponding Tafel slopes. (c) Nyquist plots measured at −0.226 V (*vs.* RHE). (d) Multistep chronopotentiometry response without iR compensation with current densities of −10, −30, −75, −100 and −150 mA cm^{-2}.

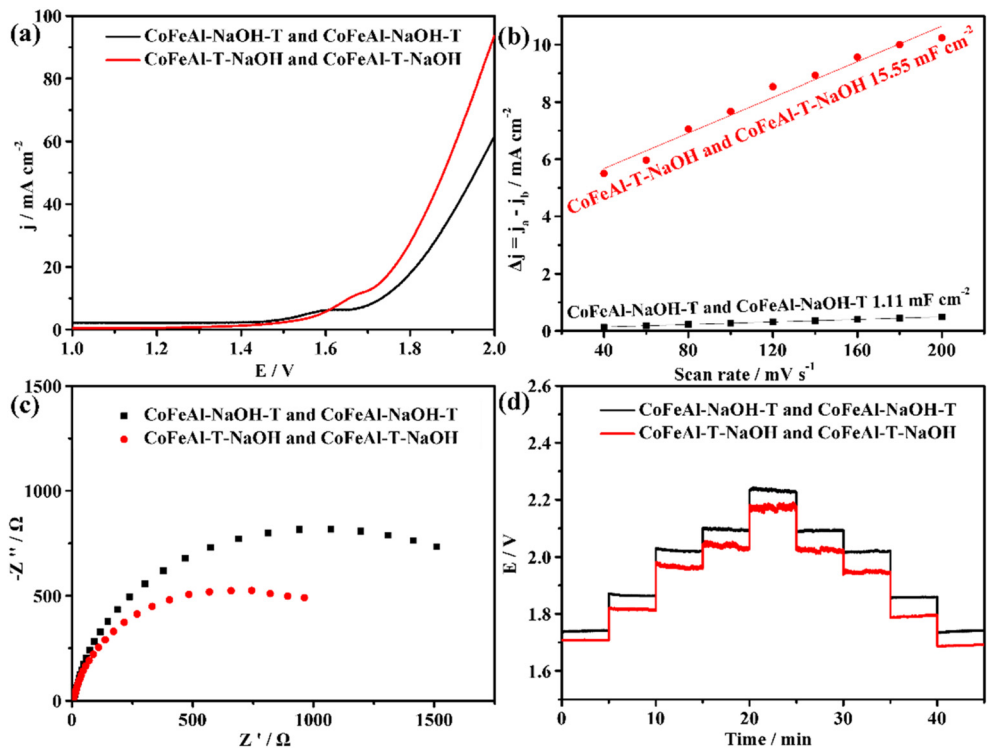

Fig. 7 Catalytic performances of the two electrodes for overall water splitting. (a) The samples were scanned by LSV measurements at a scan rate of 10 mV s^{-1} without iR compensation. (b) The relationship between the current density difference Δ*j* and the scan rate. (c) Nyquist plots measured at 1.352 V (*vs.* RHE). (d) Multistep chronopotentiometry response without iR compensation with current densities of 10, 30, 75, 100 and 150 mA cm^{-2}.

 This journal is © The Royal Society of Chemistry 2023

Published on 25 abril 2023. Downloaded on 06/07/2024 19:31:19.

curves plotted in Fig. 6b show the smallest value of 106.5 mV dec^{-1} for CoFeAl-T-NaOH, illustrating its fast reaction kinetics for HER among the prepared electrocatalysts. The electrochemical impedance spectra also exhibit the smallest charge transfer resistance for CoFeAl-T-NaOH (Fig. 6c), revealing its fast charge transfer capability. Fig. 6d depicts the fast chronopotentiometry response from −10 to −150 mA cm^{-2} without a fluctuation for each step, further manifesting the excellent mass transport and charge transfer performance. In addition, the long-term stability of these catalysts was evaluated by chronopotentiometric analysis, as shown in Fig. SI8.† The CoFeAl-T-NaOH remained steady without obvious fluctuation at 150 mA cm^{-2} (Fig. SI8†). All these results point to the fact that CoFeAl-T-NaOH possesses an excellent HER performance among these catalysts.

3.4. Overall water splitting

With the excellent OER and HER activities of CoFeAl-T-NaOH in hand, a two-electrode system was assembled with CoFeAl-T-NaOH serving as both anode and cathode for the overall water splitting and the CoFeAl-NaOH-T was used as a control sample. From the LSV curve of the overall water splitting in Fig. 7a, the CoFeAl-T-NaOH catalyst only requires a cell voltage of 1.65 V to reach 10 mA cm^{-2}, which is lower than that of CoFeAl-NaOH-T (1.73 V). The ECSAs of the CoFeAl-T-NaOH and CoFeAl-NaOH-T were evaluated to be 15.55 and 1.11 mF cm^{-2}, respectively (Fig. 7b and Fig. SI9a, b†). Moreover, the EIS shows the lower charge transfer resistance of CoFeAl-T-NaOH than that of CoFeAl-NaOH-T, which is favorable for charge transfer (Fig. SI7c†). The fast multistep chronopotentiometry responses (Fig. 7d) and long-term stability (Fig. SI9c†) both verify that the CoFeAl-T-NaOH catalyst possesses an excellent mass transport and charge transfer performance, as well as the robustness of the electrode for overall water electrolysis. Taken together, CoFeAl-T-NaOH shows a superior electrocatalytic performance to that of CoFeAl-NaOH-T, due to the effect of the sequence of NaOH etching and the sulfidation process on the catalytic properties of the CoFeAl LDH evolved catalysts.

4. Conclusions

In summary, the hierarchically interconnected porous CoFeAl-T-NaOH catalyst was successfully synthesized from CoFeAl LDH by a sulfidation and NaOH etching process. The as-prepared CoFeAl-T-NaOH catalyst exhibits an excellent OER and HER catalytic activity and long-term robustness at room temperature in 1.0 M KOH. Moreover, serving as both cathode and anode electrode for overall water splitting, the CoFeAl-T-NaOH catalyst shows a relatively lower cell voltage to deliver a 10 mA cm^{-2} current and excellent stability at the large current density. The hierarchically interconnected nanosheets, porous structure, metal (Fe, Co and Ni) sulfide heterojunctions and synergetic effect effectively facilitate the electrolyte infiltration, charge transfer and mass transport during the electrocatalytic process, and are responsible for the enhanced electrocatalytic activity.

Conflicts of interest

There are no conflicts to declare.

Acknowledgements

This work has received funding from the Natural science Research Fund for Colleges and Universities in Anhui Province (no. KJ2021A0387, KJ2019A0049), Natural Science Foundation of Anhui Province of China (grant no. 2108085MB35), the Scientific Research Foundation of the Education Department of Anhui Province of China (no. KJ2021ZD0043), Introduction and Cultivation Plan of Young Innovative Talents in Colleges and Universities of Shandong Province, the Natural Science Foundation of Shandong Province (grant no. ZR2020ME052), and the Joint Fund of the Yulin University and the Dalian National Laboratory for Clean Energy (grant YLU-DNL Fund 2021001).

References

1 Z. W. Seh, J. Kibsgaard, C. F. Dickens, I. Chorkendorff, J. K. Nørskov and T. F. Jaramillo, Combining theory and experiment in electrocatalysis: insights into materials design, *Science*, 2017, **355**, eaad4998.
2 F. Dionigi, Z. H. Zeng, I. Sinev, T. S. Merzdorf, S. Deshpande, M. B. Lopez, S. Kunze, I. Zegkinoglou, H. Sarodnik, D. X. Fan, A. Bergmann, J. Drnec, J. F. Araujo, M. Gliech, D. Teschner, J. Zhu, W.-X. Li, J. Greeley, B. R. Cuenya and P. Strasser, In-situ structure and catalytic mechanism of NiFe and CoFe layered double hydroxides during oxygen evolution, *Nat. Commun.*, 2020, **11**, 2522.
3 J. Chi, H. M. Yu, B. W. Qin, L. Fu, J. Jia, B. L. Yi and Z. G. Shao, Vertically aligned FeOOH/NiFe layered double hydroxides electrode for highly efficient oxygen evolution reaction, *ACS Appl. Mater. Interfaces*, 2017, **9**, 464–471.
4 J. D. Chen, F. Zheng, S. J. Zhang, A. Fisher, Y. Zhou, Z. Y. Wang, Y. Y. Li, B. B. Xu, J. T. Li and S. G. Sun, Interfacial interaction between FeOOH and Ni-Fe LDH to modulate the local electronic structure for enhanced OER electrocatalysis, *ACS Catal.*, 2018, **8**, 11342–11351.
5 T. T. Wang, Y. Zhang, Y. Q. Wang, J. N. Zhou, L. Q. Wu, Y. Sun, X. B. Xu, W. T. Hou, X. Zhou, Y. W. Du and W. Zhong, Alumina-supported CoPS nanostructures derived from LDH as highly active bifunctional catalysts for overall water splitting, *ACS Sustainable Chem. Eng.*, 2018, **6**, 10087–10096.
6 K. A. Sun, X. Y. Wu, Z. W. Zhuang, L. Y. Liu, J. J. Fang, L. Y. Zeng, J. G. Ma, S. J. Liu, J. Z. Li, R. Y. Dai, X. Tan, K. Yu, D. Liu, W.-C. Cheong, A. J. Huang, Y. Q. Liu, Y. Pan,

Published on 25 abril 2023. Downloaded on 06/07/2024 19:31:19.

H. Xiao and C. Chen, Interfacial water engineering boosts neutral water reduction, *Nat. Commun.*, 2022, **13**, 6260.

7 T. Y. Zhang, J. Jin, J. M. Chen, Y. Y. Fang, X. Han, J. Y. Chen, Y. P. Li, Y. Wang, J. F. Liu and L. Wang, Pinpointing the axial ligand effect on platinum single-atom-catalyst towards efficient alkaline hydrogen evolution reaction, *Nat. Commun.*, 2022, **13**, 6875.

8 S. D. Liu, H. K. Li, J. Zhong, K. Xu, G. Wu, C. Liu, B. B. Zhou, Y. Yan, L. X. Li, W. H. Cha, K. K. Chang, Y. Y. Li and J. Lu, A crystal glass–nanostructured Al-based electrocatalyst for hydrogen evolution reaction, *Sci. Adv.*, 2022, **8**, eadd6421.

9 F.-Y. Gao, S.-N. Liu, J.-C. Ge, X.-L. Zhang, L. Zhu, Y.-R. Zheng, Y. Duan, S. Qin, W. X. Dong, X. X. Yu, R.-C. Bao, P.-P. Yang, Z.-Z. Niu, Z.-G. Ding, W. Liu, S. Lan, M.-R. Gao, Y. S. Yan and S.-H. Yu, Nickel–molybdenum–niobium metallic glass for efficient hydrogen oxidation in hydroxide exchange membrane fuel cells, *Nat. Catal.*, 2022, **5**, 993–1005.

10 X. P. Wang, S. B. Xi, P. R. Huang, Y. H. Du, H. Y. Zhong, Q. Wang, A. Borgna, Y.-W. Zhang, Z. B. Wang, H. Wang, Z. G. Yu, W. S. V. Lee and J. M. Xue, Pivotal role of reversible NiO_6 geometric conversion in oxygen evolution, *Nature*, 2022, **611**, 702–708.

11 L. B. Sun, V. Reddu and X. Wang, Multi-atom cluster catalysts for efficient electrocatalysis, *Chem. Soc. Rev.*, 2022, **51**, 8923–8956.

12 X. Long, Z. L. Wang, S. Xiao, Y. M. An and S. H. Yang, Transition metal based layered double hydroxides tailored for energy conversion and storage, *Mater. Today*, 2016, **19**, 213–226.

13 F. Xian, L. L. Jia, Y. Sugahara, H. R. Xue, Y. Yamauchi, T. Sasaki and R. Z. Ma, Constructing fast transmembrane pathways in a layered double hydroxide nanosheets/nanoparticles composite film for an inorganic anion-exchange membrane, *ACS Appl. Mater. Interfaces*, 2022, **14**, 51212–51221.

14 L. Qian, Z. Lu, T. Xu, X. Wu, Y. Tian, Y. Li, Z. Huo, X. Sun and X. Duan, Trinary layered double hydroxides as high-performance bifunctional materials for oxygen electrocatalysis, *Adv. Energy Mater.*, 2015, **5**, 1500245.

15 X. Jia, S. Gao, T. Liu, D. Li, P. Tang and Y. Feng, *Electrochim. Acta*, 2017, **245**, 59–68.

16 X. L. Deng, J. Z. Huang, H. Wan, F. S. Chen, Y. F. Lin, X. J. Xu, R. Z. Ma and T. Sasaki, Recent progress in functionalized layered double hydroxides and their application in efficient electrocatalytic water oxidation, *J. Energy Chem.*, 2019, **32**, 93–104.

17 F. Huang, B. Q. Yao, Y. Z. Huang and Z. L. Dong, NiFe layered double hydroxide nanosheet arrays for efficient oxygen evolution reaction in alkaline media, *Int. J. Hydrogen Energy*, 2022, **47**, 21725–21735.

18 L. Wang, L. Zhang, W. Ma, H. Wan, X. Zhang, X. Zhang, S. Jiang, J. Y. Zheng and Z. Zhou, In situ anchoring massive isolated Pt atoms at cationic vacancies of α-$Ni_xFe_{1-x}(OH)_2$ to regulate the electronic structure for overall water splitting, *Adv. Funct. Mater.*, 2022, **32**, 2203342.

19 J. Ge, J. Y. Zheng, J. Zhang, S. Jiang, L. Zhang, H. Wan, L. Wang, W. Ma, Z. Zhou and R. Ma, Controllable atomic defect engineering in layered $Ni_xFe_{1-x}(OH)_2$ nanosheets for electrochemical overall water splitting, *J. Mater. Chem. A*, 2021, **9**, 14432–14443.

20 S. Zhang, Y. Zhang, W. Jiang, X. Liu, S. Xu, R. Huo, F. Zhang and J. Hu, Co@N-CNTs derived from triple-role CoAl-layered double hydroxide as an efficient catalyst for oxygen reduction reaction, *Carbon*, 2016, **107**, 162–170.

21 X. Jia, S. Gao, T. Liu, D. Li, P. Tang and Y. Feng, Fabrication and bifunctional electrocatalytic performance of ternary CoNiMn layered double hydroxides/polypyrrole/reduced graphene oxide composite for oxygen reduction and evolution reactions, *Electrochim. Acta*, 2017, **245**, 59–68.

22 H. J. Yan, Y. Xie, A. P. Wu, Z. C. Cai, L. Wang, C. G. Tian, X. M. Zhang and H. G. Fu, Anion-modulated HER and OER activities of 3D Ni-V-based interstitial compound heterojunctions for high-efficiency and stable overall water splitting, *Adv. Mater.*, 2019, **31**, 1901174.

23 S. S. Wang, Y. Liu, X. L. Deng, J. F. Cao, Y. F. Han, J. Z. Huang and Y. B. Li, Co_3S_4/Fe_3S_4 heterostructured bifunctional catalyst evolved from CoFe LDH for effective overall water splitting in alkaline solution, *J. Alloys Compd.*, 2022, **925**, 166787.

24 C. Zhang, Y. Shi, Y. Yu, Y. Du and B. Zhang, Engineering sulfur defects, atomic thickness, and porous structures into cobalt sulfide nanosheets for efficient electrocatalytic alkaline hydrogen evolution, *ACS Catal.*, 2018, **8**, 8077–8083.

25 Y. Zhou, M. Luo, Z. Zhang, W. Li, X. Shen, W. Xia, M. Zhou and X. Zeng, Iron doped cobalt sulfide derived boosted electrocatalyst for water oxidation, *Appl. Surf. Sci.*, 2018, **448**, 9–15.

26 A. Wang, M. Zhang, H. Li, F. Wu, K. Yan and J. Xiao, Combination of theory and experiment achieving a rational design of electrocatalysts for hydrogen evolution on the hierarchically mesoporous CoS_2 microsphere, *J. Phys. Chem. C*, 2019, **123**, 13428–13433.

27 R. Miao, B. Dutta, S. Sahoo, J. He, W. Zhong, S. A. Cetegen, T. Jiang, S. P. Alpay and S. L. Suib, Mesoporous iron sulfide for highly efficient electrocatalytic hydrogen evolution, *J. Am. Chem. Soc.*, 2017, **139**, 13604–13607.

28 C. Kim, S. H. Kim, S. Lee, I. Kwon, S. Kim, C. Seok, Y. S. Park and Y. Kim, Boosting overall water splitting by incorporating sulfur into NiFe (oxy)hydroxide, *J. Energy Chem.*, 2022, **64**, 364–371.

29 H. Wen, Z. Y. Yi, Z. Y. Hu, R. Guo and X. W. Liu, Design strategy for low-temperature sulfur etching to achieve high-performance hollow multifunctional electrode material, *J. Mater. Sci. Technol.*, 2022, **119**, 209–218.

30 Y. F. Zeng, L. J. Chen, R. Chen, Y. Y. Wang, C. Xie, L. Tao, L. L. Huang and S. Y. Wang, One-step, room temperature generation of porous and amorphous cobalt hydroxysulfides from layered double hydroxides for superior oxygen evolution reactions, *J. Mater. Chem. A*, 2018, **6**, 24311–24316.

 This journal is © The Royal Society of Chemistry 2023

Published on 25 abril 2023. Downloaded on 06/07/2024 19:31:19.

31 Y. F. Zeng, Y. Y. Wang, G. Huang, C. Chen, L. L. Huang, R. Chen and S. Y. Wang, Porous CoP nanosheets converted from layered double hydroxides with superior electrochemical activity for hydrogen evolution reactions at wide pH ranges, *Chem. Commun.*, 2018, **54**, 1465–1468.

32 C. Janson and A. E. C. Palmqvist, Improved oxygen reduction activity of transition metal-chelating ordered mesoporous carbon fuel cell catalysts by milder template removal, *Catal. Lett.*, 2019, **149**, 1297–1304.

33 J. S. Yang, C. Li, D. R. Liang, Y. Liu, Z. S. Li, H. Y. Wang, H. H. Huang, C. F. Xia, H. Zhao, Y. Y. Liu, Q. Zhang and Z. L. Meng, Central-collapsed structure of CoFeAl layered double hydroxides and its photocatalytic performance, *J. Colloid Interface Sci.*, 2021, **590**, 571–579.

34 B. Quan, X. H. Liang, G. B. Ji, J. Lv, S. S. Dai, G. Y. Xu and Y. W. Du, Laminated graphene oxide-supported high-efficiency microwave absorber fabricated by an in situ growth approach, *Carbon*, 2018, **129**, 310–320.

35 S. Lee, M. Govindan and D. Kim, CoFe-based layered double hydroxide for high removal capacity of hydrogen sulfide under high humid gas stream, *Chem. Eng. J.*, 2020, **416**, 127918.

36 C. Tang, Z. H. Pu, Q. Liu, A. M. Asiri, Y. L. Luo and X. P. Sun, Ni_3S_2 nanosheets array supported on Ni foam: A novel efficient three-dimensional hydrogen-evolving electrocatalyst in both neutral and basic solutions, *Int. J. Hydrogen Energy*, 2015, **40**, 4727–4732.

37 C. Fan, X. P. Shen, J. Cheng, L. M. Lang, G. X. Liu, Z. Y. Ji and G. X. Zhu, One-pot synthesis of Ni_3S_2/Co_3S_4/FeOOH flower-like microspheres on Ni foam: an efficient binder-free bifunctional electrode towards overall water splitting, *Colloids Surf., A*, 2021, **631**, 127689.

38 S. H. Wang, T. Y. Wang, X. L. Kong, X. D. Zhao, H. Y. Gan, X. X. Wang, Q. J. Meng, F. He, P. P. Yang and Z. L. Liu, Ultrafine aluminum sulfide nanocrystals anchored on two-dimensional carbon sheets for high-performance lithium-ion batteries, *J. Colloid Interface Sci.*, 2023, **630**, 204–211.

39 A. Mehmood, G. Rahman, A. u. H. A. Shah, O.-S. Joo and S. A. Mian, Template-free hydrothermal growth of nickel sulfide nanorods as high-performance electroactive materials for oxygen evolution reaction and supercapacitors, *Energy Fuels*, 2021, **35**, 6868–6879.

40 C. You, Y. Y. Ji, Z. Liu, X. L. Xiong and X. P. Sun, Ultrathin CoFe-borate layer coated CoFe-layered double hydroxide nanosheets array: A non-noble-metal 3D catalyst electrode for efficient and durable water oxidation in potassium borate, *ACS Sustainable Chem. Eng.*, 2018, **6**, 1527–1531.

41 L. X. Zhou, M. C. Guo, Y. Li, Q. Gu, W. Q. Zhang, C. Li, F. Y. Xie, D. M. Lin and Q. J. Zheng, One-step synthesis of wire-in-plate nanostructured materials made of CoFe-LDH nanoplates coupled with $Co(OH)_2$ nanowires grown on a Ni foam for a high-efficiency oxygen evolution reaction, *Chem. Commun.*, 2019, **55**, 4218.

42 X. T. Han, C. Yu, S. Zhou, C. T. Zhao, H. W. Huang, J. Yang, Z. B. Liu, J. J. Zhao and J. S. Qiu, Ultrasensitive iron-triggered nanosized Fe-CoOOH integrated with graphene for highly efficient oxygen evolution, *Adv. Energy Mater.*, 2017, **7**, 1602148.

43 Z. F. Huang, J. Song, Y. Du, S. Xi, S. Dou, J. M. V. Nsanzimana, C. Wang, Z. J. Xu and X. Wang, Chemical and structural origin of lattice oxygen oxidation in Co–Zn oxyhydroxide oxygen evolution electrocatalysts, *Nat. Energy*, 2019, **4**, 328–338.

44 L. N. Ma, H. Zhou, M. Xu, P. P. Hao, X. G. Kong and H. H. Duan, Integrating hydrogen production with anodic selective oxidation of sulfides over a CoFe layered double hydroxide electrode, *Chem. Sci.*, 2021, **12**, 938–945.

45 F. Z. Sun, C. Q. Li, B. Li and Y. Q. Lin, Amorphous MoS_x developed on $Co(OH)_2$ nanosheets generating efficient oxygen evolution catalysts, *J. Mater. Chem. A*, 2017, **5**, 23103–23114.

46 D. Merki, H. Vrubel, L. Rovelli, S. Fierro and X. L. Hu, Fe, Co, and Ni ions promote the catalytic activity of amorphous molybdenum sulfide films for hydrogen evolution, *Chem. Sci.*, 2012, **3**, 2515–2525.

47 X. Y. Lu and C. Zhao, Electrodeposition of hierarchically structured three-dimensional nickel–iron electrodes for efficient oxygen evolution at high current densities, *Nat. Commun.*, 2015, **6**, 6616.

48 R. Duan, Y. J. Li, S. Gong, Y. G. Tong, Z. Li and W. H. Qi, Hierarchical CoFe oxyhydroxides nanosheets and Co_2P nanoparticles grown on Ni foam for overall water splitting, *Electrochim. Acta*, 2020, **360**, 136994.

49 L. Hu, T. Z. Xiong, R. Liu, Y. W. Hu, Y. C. Mao, M.-S. Balogun and Y. X. Tong, Co_3O_4@Cu-based conductive metal–organic framework core–shell nanowire electrocatalysts enable efficient low-overall-potential water splitting, *Chem. – Eur. J.*, 2019, **25**, 6575–6583.